Domain orientations and piezoelectric properties in novel 2–2-type composites with two single-crystal components

V. Yu. Topolov,[a] A. V. Krivoruchko,[b] C. R. Bowen,[c] and A. A. Panich[d]

[a]Department of Physics, Southern Federal University, 344090 Rostov-on-Don, Russia

[b]Don State Technical University, 344000 Rostov-on-Don, Russia

[c]Department of Mechanical Engineering, University of Bath, Bath BA2 7AY, UK

[d]Institute of High Technologies and Piezotechnics, Southern Federal University, 344090 Rostov-on-Don, Russia

The present paper is concerned with the piezoelectric properties and related parameters of the 2–2-type parallel-connected composites wherein rotations of the main crystallographic axes in ferroelectric single-crystal components are analysed. The composite consists of layers of two types that are regularly arranged along the non-polar axis. The Type I layer is a single-domain $0.63Pb(Mg_{1/3}Nb_{2/3})O_3–0.37PbTiO_3$ single crystal (either tetragonal in Composite I or orthorhombic in Composite II). The Type II layer is a $Li_2B_4O_7$ single crystal / polyethylene medium with 0–3 connectivity. The composite as a whole is characterised by 2–0–2 connectivity, and the following parameters of the composite are studied by taking into account the polarisation orientation effect in the Type I layer and the microgeometry of the composite in the Type II layer: piezoelectric coefficients d_{3j}^* and g_{3j}^* and their hydrostatic analogs d_h^* and g_h^*, hydrostatic squared figure of merit $d_h^* g_h^*$, and piezoelectric anisotropy factors d_{33}^*/d_{32}^* and d_{33}^*/d_{32}^*. It is shown that large values of the studied piezoelectric coefficients, hydrostatic parameters and anisotropy factors make Composite II more preferable in comparison to Composite I for hydroacoustic, piezoelectric sensor and energy-harvesting applications.

Keywords Piezo-active composite based on relaxor-ferroelectric; Piezoelectric properties; Orientation effect; Hydrostatic parameters; Anisotropy factors

PACS 77.65.-j: Piezoelectricity and electromechanical effects; 77.84.Lf: Composite materials; and 77.84.-s: Dielectric; piezoelectric; ferroelectric; and antiferroelectric materials

Running head: **Domain Orientations and Piezoelectric Properties**

Contact V. Yu. Topolov vutopolov@sfedu.ru

1. Introduction

Single crystals (SCs) of relaxor-ferroelectric $(1 - x)Pb(Mg_{1/3}Nb_{2/3})O_3–xPbTiO_3$ (PMN–*x*PT) are advanced piezoelectric materials that exhibit outstanding electromechanical properties [1, 2] near the morphotropic phase boundary. Large piezoelectric coefficients d_{ij} in these SCs are achieved at poling along specific crystallographic directions (e.g. [001], [011] or [111] in the perovskite unit-cell axes), due to the formation of domain-engineered structures and owing to intermediate phases of the ferroelectric nature [3, 4]. The PMN–*x*PT SCs are often regarded as highly effective components of modern piezo-active composites [5–8] that are suitable in hydroacoustic, piezoelectric sensor, transducer, and energy-harvesting applications. In the last 15 years, full sets of electromechanical constants have been measured for about ten compositions of the poled PMN–*x*PT SCs being either single-domain [4, 9–11] or domain-engineered [3, 10, 12]. Among these compositions, of specific interest is the PMN–0.37PT SC for which two sets of electromechanical constants have been found at room temperature [4, 11]. According to work [11], the [001]-poled single-domain PMN–0.37PT SC is related to the tetragonal 4*mm* symmetry class, and the full set of electromechanical constants is shown in the 2nd column of Table 1. As is known from experimental results [4], at the electric field $\boldsymbol{E} \parallel [011]$, the following phase sequence is observed: tetragonal (4*mm* symmetry) → monoclinic M_C (*m* symmetry) → single-domain orthorhombic (*mm*2 symmetry). Hereby the field-induced phase transitions on increasing *E* are observed at $E \approx 4$ kV / cm (tetragonal → M_C) and 6 kV / cm (M_C → orthorhombic). The spontaneous polarisation vector $\boldsymbol{P_s}$ in the single-domain state is oriented as $\boldsymbol{P_s} \parallel [001]$ (tetragonal phase) or $\boldsymbol{P_s} \parallel [011]$ (orthorhombic phase). On decreasing *E* from its maximum value, the single-domain orthorhombic phase is maintained at $E \geq 3.5$ kV / cm. A further decrease in *E* from 3.5 kV / cm to 0 kV / cm leads to the transition to the intermediate M_C phase and then to a coexistence of the M_C and tetragonal phases [4]. The full set of electromechanical constants of the single-domain PMN–0.37PT SC in the orthorhombic phase is given in the 3rd column of Table 1.

A relatively simple 2–2-type composite architecture (i.e., a system of alternating layers), its modifications [13–16], and polarisation orientation effects [6, 15] can be considered in order to compare the piezoelectric performance of the similar composites that are based on either the PMN–0.37PT SC in the tetragonal phase or the PMN–0.37PT SC in the orthorhombic phase. In addition, recent studies on the 2–2-type composites with two SC components [16] show that such composites are of interest due to the set of large parameters that characterise the piezoelectric anisotropy, sensitivity, electromechanical coupling, and hydrostatic piezoelectric response. The aim of the present paper is

(i) to analyse the influence of the PMN–0.37PT SC on the piezoelectric properties and related hydrostatic parameters of the 2–2-type composites and

(ii) to compare the performance of the composite based on the [001]-poled PMN–0.37PT SC to the performance of the related composite based on the [011]-poled PMN–0.37PT SC.

2. Model of the 2–2-type composite and its effective electromechanical properties

2.1. Model concepts

It is assumed that the composite consists of a system of parallel-connected layers of two types (*Type I* and *Type II* layers, Fig. 1) with interfaces that are parallel to the (X_2OX_3) plane. The Type I and Type II layers are regularly arranged along the coordinate OX_1 axis. The Type I layer is the PMN–0.37PT SC and is characterised by a spontaneous polarisation $\boldsymbol{P}_s^{(1)}$ and volume fraction m in the whole composite sample. The crystallographic axes X, Y, and Z in each Type I layer are oriented uniformly; for instance, in the [001]-poled SC, conditions $X \parallel OX_1$, $Y \parallel OX_2$, and $Z \parallel OX_3$ hold. The Type II layer is a SC / polymer medium with 0–3 connectivity in terms of work [6, 8, 17], and the volume fraction of the Type II layers is $1 - m$ (Fig. 1). The shape of each SC inclusion in the Type II layer is spheroidal and obeys the equation $(x_1 / a_1)^2 + (x_2 / a_2)^2 + (x_3 / a_3)^2 = 1$ in the coordinate OX_f axes. Hereafter the shape of the SC inclusion is described in terms of the aspect ratio $\rho_i = a_1 / a_3$, and the volume fraction of the SC inclusions over the Type II layers is

m_i. The SC inclusions in the polymer medium are considered on assumption that the linear sizes of each SC inclusion are much smaller than the thickness of each layer of the sample shown in Fig. 1. The spheroidal SC inclusions occupy sites of a simple tetragonal lattice with unit-cell vectors parallel to the OX_f axes, where f = 1, 2, and 3. The orientation of the crystallographic axes X, Y and Z of each SC inclusion in the Type II layer is given by $X \parallel OX_1$, $Y \parallel OX_2$ and $Z \parallel OX_3$. The composite shown in Fig. 1 is characterised by 2–0–2 connectivity where the first index '2' refers to the SC component in the Type I layer, the index '0' is related to the SC component in the Type II layer, and the last index '2' is written for the polymer component in the Type II layer.

The polarisation orientation effect in the composite is caused by a rotation of the spontaneous polarisation vector $\boldsymbol{P}_s^{(1)}$ (and therefore, the main crystallographic axes X, Y and Z) in each Type I layer. By analogy with work [6, 15], the orientation of $\boldsymbol{P}_s^{(1)}$ in each Type I layer is described by the Euler angles φ, ψ, and θ, see Fig. 1. At φ = ψ = θ = 0°, the $\boldsymbol{P}_s^{(1)}$ vector is parallel to [001] of the perovskite unit cell ([001]-poled SC, 4*mm* symmetry) or to [011] of the perovskite unit cell ([011]-poled SC, *mm*2 symmetry), and the $\boldsymbol{P}_s^{(1)}$ orientation is connected with the coordinate system ($X_1^o X_2^o X_3^o$). In fact, ($X_1^o X_2^o X_3^o$) is the crystallographic coordinate system of the single-domain SC. After the rotation of the main crystallographic axes in each Type I layer, conditions $X \parallel OX_1'$, $Y \parallel OX_2'$, and $Z \parallel OX_3'$ hold. The transition from ($X_1^o X_2^o X_3^o$) to ($X_1'X_2'X_3'$) (Fig. 1) is described by the rotation matrix [6]

$$\left\| r \right\| = \begin{pmatrix} \cos\psi\cos\varphi - \sin\psi\cos\theta\cos\varphi & \cos\psi\sin\varphi + \sin\psi\cos\theta\cos\varphi & \sin\psi\sin\theta \\ -\sin\psi\cos\varphi - \cos\psi\cos\theta\sin\varphi & -\sin\psi\sin\varphi + \cos\psi\cos\theta\cos\varphi & \cos\psi\sin\theta \\ \sin\theta\sin\varphi & -\sin\theta\cos\varphi & \cos\theta \end{pmatrix}. \quad (1)$$

In the present paper, we analyse the piezoelectric properties and related parameters of two composites as follows. The term '*Composite I*' is introduced for the 2–2-type composite based on the [001]-poled PMN–0.37PT SC, and the term '*Composite II*' is related to the 2–2-type composite based on the [011]-poled PMN–0.37PT SC. In both these composites, the polarisation

orientation effect is considered. It should be added that the single-domain state in the composites can be maintained by an external bias field [4, 11] applied along the specific direction.

2.2. Effective electromechanical properties

Effective electromechanical properties of the 2–0–2 composite shown in Fig. 1 can be evaluated in three stages as follows. During the first stage, we evaluate the effective properties of the Type II layer, i.e., the 0–3 SC / polymer composite. These effective properties are determined by means of the effective field method [6, 8] that takes into account an interaction between the piezoelectric SC inclusions. We assume that the components in the Type II layer are characterised by elastic moduli $c_{ab}^{(SC),E}$ (SC inclusions) and $c_{ab}^{(p),E}$ (polymer matrix), piezoelectric coefficients $e_{ij}^{(SC)}$ (SC inclusions) and $e_{ij}^{(p)}$ (polymer matrix), and dielectric permittivities $\varepsilon_{qq}^{(SC),\xi}$ (SC inclusions) and $\varepsilon_{qq}^{(p),\xi}$ (polymer matrix). The effective electromechanical properties of the Type II layer are represented in the form of the 9 × 9 matrix as follows:

$$\| C^{(2)} \| = \begin{pmatrix} \| c^{(2),E} \| & \| e^{(2)} \|^t \\ \| e^{(2)} \| & -\| \varepsilon^{(2),\xi} \| \end{pmatrix}. \qquad (2)$$

In Eq. (2), the superscript t denotes the transposition. Elements of $\| C^{(2)} \|$ are calculated within the framework of the effective field method [6, 8], and the main formula of the effective properties of the 0–3 composite is given by

$$\| C^{(2)} \| = \| C^{(p)} \| + m_i (\| C^{(SC)} \| - \| C^{(p)} \|)[\| I \| + (1 - m_i)\| S \| \cdot \| C^{(p)} \|^{-1} (\| C^{(SC)} \| - \| C^{(p)} \|)]^{-1}. \qquad (3)$$

In Eq. (3), $\| C^{(SC)} \|$ and $\| C^{(p)} \|$ are matrices of the properties of the SC and polymer components, respectively, m_i is the volume fraction of the SC-2 component in the Type II layer, $\| I \|$ is the identity matrix, and $\| S \|$ is the matrix that contains the Eshelby tensor components [18]. The $\| S \|$ matrix depends on elements of $\| C^{(p)} \|$ and the aspect ratio ρ_i of the SC inclusion. The $\| C^{(SC)} \|$ and $\| C^{(p)} \|$ matrices from Eq. (3) have the form similar to that shown in Eq. (2).

In the second stage, the elastic, piezoelectric, and dielectric properties of the Type I layer are determined by taking into account the $\boldsymbol{P_s^{(1)}}$ orientation. These properties depend on the Euler angles φ, ψ, and θ, and elements of the $\| r \|$ matrix from Eq. (1) are used at this determination.

The third stage is concerned with the evaluation of the effective electromechanical properties of the 2–0–2 composite as a whole. Hereby we apply the matrix method [6, 8] that allows for the electromechanical interaction between the Type I and Type II layers shown in Fig. 1. The electromechanical properties of the Type I and Type II layers are represented in the general form as

$$|| C^{(n)}|| = \begin{pmatrix} || s^{(n),E} || & || d^{(n)} ||^t \\ || d^{(n)} || & || \varepsilon^{(n),\sigma} || \end{pmatrix}. \quad (4)$$

In Eq. (3), $|| C^{(n)}||$ is the 9 × 9 matrix, $n = 1$ is related to the Type I layer, and $n = 2$ refers to the Type II layer, $|| s^{(n),E} ||$ is the 6 × 6 matrix of elastic compliances, $|| d^{(n)} ||$ is the 3 × 6 matrix of piezoelectric coefficients, $|| \varepsilon^{(n),\sigma} ||$ is the 3 × 3 matrix of dielectric permittivities, and the superscript t denotes the transposition. A transition from the matrix elements of the Type II layer in the form of Eq. (3) to the matrix elements in the form of Eq. (4) is carried out using conventional formulae [19] for the piezoelectric medium. Finally, the matrix of the effective electromechanical properties of the 2–0–2 composite is written [6, 8] as

$$|| C^* || = [|| C^{(1)} ||\cdot|| M || m + || C^{(2)} || (1 - m)] [|| M || m + || I || (1 - m)]^{-1}. \quad (5)$$

The structure of the $|| C^* ||$ matrix from Eq. (5) is shown in Eq. (4). In Eq. (5), $|| C^{(1)} ||$ and $|| C^{(2)} ||$ are taken from Eq. (4), $|| M ||$ is concerned with boundary conditions at the interface x_1 = const (Fig. 1), and $|| I ||$ is the identity matrix. The boundary conditions [6] at x_1 = const imply a continuity of components of mechanical stress σ_{11}, σ_{12} and σ_{13}, strain ξ_{22}, ξ_{23} and ξ_{33}, electric displacement D_1, and electric field E_2 and E_3.

In a general case, the $|| C^* ||$ matrix from Eq. (5) is to be analysed as a function of six variables, i.e., $|| C^* || = || C^*(m, \rho_i, m_i, \varphi, \psi, \theta) ||$. Based on the matrix elements of $|| C^* ||$ from Eq. (5), we find the piezoelectric coefficients g_{ij}^* by using the relation [6, 19] $|| g^* || = || \varepsilon^{*\sigma} ||^{-1}\cdot|| d^* ||$. In the present paper, we analyse the following effective parameters of the 2–0–2 composite:

(i) piezoelectric coefficients d_{3j}^* and g_{3j}^* and their hydrostatic analogs

$$d_h^* = d_{33}^* + d_{32}^* + d_{31}^* \text{ and } g_h^* = g_{33}^* + g_{32}^* + g_{31}^*, \quad (6)$$

(ii) hydrostatic squared figure of merit

$$(Q_h^*)^2 = d_h^* g_h^*, \quad (7)$$

and

(iii) piezoelectric anisotropy factors

$$\zeta_{d1} = d_{33}^* / d_{31}^* \text{ and } \zeta_{d2} = d_{33}^* / d_{32}^*. \quad (8)$$

Eqs. (6) are written for a case when electrodes applied to the composite sample shown in Fig. 1 are perpendicular to the OX_3 axis. The hydrostatic squared figure of merit $(Q_h^*)^2$ from Eq. (7) is used to estimate the sensor signal-to-noise ratio of the piezoelectric material and, therefore, an important parameter for hydroacoustic and energy-harvesting applications [6, 8]. The anisotropy factors ζ_{d1} and ζ_{d2} from Eqs. (8) can be taken into account in sensor, acoustic, and energy-harvesting applications [6].

Our further evaluations are carried out by using the full sets of electromechanical constants of the components, see Tables 1 and 2. We note the considerable elastic anisotropy of the PMN–0.37PT SC and appreciable changes in the piezoelectric coefficients d_{ij} at the change of the poling direction [001] $\rightarrow$ [011], see data in Table 1. We consider a piezoelectric $Li_2B_4O_7$ (LBO) SC as an inclusion material in the polymer medium in the Type II layer, and monolithic polyethylene as a matrix material in the Type II layer. As follows from Table 2, the LBO SC is a highly original lead-free piezoelectric component because

(i) the symmetry of the LBO SC coincides with the symmetry of the [001]-poled SC in the Type I layer,

(ii) the signs of the piezoelectric coefficients e_{ij} of the LBO SC coincide with the signs of e_{ij} of the highly anisotropic $PbTiO_3$-type ceramics [23]; however the piezoelectric effect in the LBO SC is weaker than that in the poled $PbTiO_3$-type ceramics, and

(iii) the LBO SC exhibits considerable elastic anisotropy, and the large ratio c_{13}^E / c_{12}^E ≈ 9.4 has no analogies with other poled ferroelectric ceramics and piezoelectric SCs [6, 8, 23].

Since the LBO SC and polyethylene do not exhibit ferroelectric properties [20–22], no poling of the Type II layer in the 2–0–2 composite shown in Fig. 1 is needed.

3. Piezoelectric properties and hydrostatic parameters

In Section 3, we show and discuss some examples of the piezoelectric performance of Composite I and Composite II. Taking into account recent results [15, 16], we consider the Type II layer as a 0–3 composite with highly oblate SC inclusions, i.e., an aspect ratio ρ_i = 100 is assumed. The presence of the LBO SC inclusions with the aspect ratio ρ_i >> 1 leads to the considerable elastic anisotropy of the 0–3 LBO SC / polyethylene composite (Table 3) and leads to large hydrostatic parameters of the 2–2-type composite due to decreasing its lateral piezoelectric response. The lateral piezoelectric response concerned with the piezoelectric coefficients d_{32}^* and d_{31}^* is affected by the elastic properties of the Type II layer, especially at the volume fraction of the Type I layer m < 0.5. The large difference between the elastic compliance $s_{33}^{(2),E}$ and $s_{11}^{(2),E}$ as well as small values of $s_{12}^{(2),E}$ and $s_{13}^{(2),E}$ in comparison to $s_{33}^{(2),E}$ (see Table 3) strongly influence a contribution from the piezoelectric coefficients d_{32}^* and d_{31}^* (or g_{32}^* and g_{31}^*) into the hydrostatic piezoelectric response from Eqs. (6). At ρ_i >> 1, this contribution becomes smaller compared to the piezoelectric coefficient d_{33}^* (or g_{33}^*), and therefore, the hydrostatic piezoelectric response of the composite depends on d_{33}^* (or g_{33}^*) to a large degree.

Examples of the piezoelectric activity of Composite I are shown in Fig. 2. The rotation of the main crystallographic axes of the SC component in the Type I layer by the Euler angle θ strongly influence the piezoelectric coefficients d_{3j}^* and d_h^* from Eqs. (6). Changes in the θ angle mean the rotation of the $\boldsymbol{P_s}^{(1)}$ vector over the whole composite sample (Fig. 1) and, therefore, influences the piezoelectric effect to a large extent. Comparing Fig. 2, a to Fig. 2, b, we note that

the piezoelectric coefficient d_h^* increases by ca. 1.5 times on increasing θ from 0° to 50°, and this is observed at the relatively small volume fraction of the LBO SC m_i = 0.10. At various θ, a contribution from the piezoelectric coefficient d_{31}^* into d_h^* from Eqs. (6) becomes minor in comparison to d_{32}^* and d_{33}^*. This is due to the presence of the interfaces x_1 = const in the composite sample, see Fig. 1. Such interfaces lead to a considerable decrease of $|d_{31}^*|$ of the composite in comparison to $|d_{31}^{(1)}|$ of the PMN–0.37PT SC being the main piezoelectric component in the composite. Taking into account data from Table 1 and Fig. 2, b, we state that d_h^* of Composite I can be larger than the hydrostatic piezoelectric coefficient $d_h^{(1)}$ = 47 pC / N of the [001]-poled PMN–0.37PT SC by about four times.

A considerable increase of both d_{33}^* and d_h^* is observed in Composite II even at the Euler angles φ = ψ = θ = 0° (Fig. 3). At the volume fraction m < 0.15 and in the presence of the Type II layer with the heavily oblate SC inclusions, the condition $d_{31}^* \approx -d_{32}^*$ holds for Composite II (see curves 1 and 2 in Fig. 3), and in accordance with Eqs. (6), this leads to $d_h^* \approx d_{33}^*$ (see curves 3 and 4 in Fig. 3). We add that $d_{33}^* \approx d_{33}^{(1)}$ at m > 0.10 due to the laminar structure of the composite wherein the SC component in the Type I layer is distributed continuously along the OX_3 axis (Fig. 1). Such an original behaviour of the piezoelectric coefficients d_{3j}^* and d_h^* from Eqs. (6) is observed in the composite based on the orthorhombic PMN–0.37PT SC whose electromechanical constants obeys conditions $d_{33}^{(1)} \approx |d_{31}^{(1)}|$, $d_{33}^{(1)} \approx 5\, d_{32}^{(1)}$, $s_{11}^{(1),E} \approx s_{33}^{(1),E}$, and $|s_{13}^{(1),E}| \approx s_{23}^{(1),E}$. To the best of our knowledge, no similar relations between the electromechanical constants were discussed in earlier papers on FE and piezoelectric materials, and no examples of the similar piezoelectric activity of composites were described in the literature.

Taking into account rotations of the main crystallographic axes by all the Euler angles (φ, ψ, and θ), we see that changes in ψ and θ influence the piezoelectric coefficients d_{33}^* and d_h^* of Composite II to a larger extent in comparison to changes in φ, see graphs in Fig. 4. This

influence is observed at the volume fraction of the PMN–0.37PT m = 0.10, i.e., there is a strong influence of the Type II layer with anisotropic elastic properties and weak piezoelectric properties. Due to the orientation effect in the Type I layer and due to the elastic anisotropy of the Type II layer in Composite II, large piezoelectric coefficients $d_{33}^{*} \approx 900$ pC / N (Fig. 4, d and e) and $d_{h}^{*} \approx$ 800–900 pC / N (Fig. 4, a and b) are achieved. We mention for comparison that in comparison with data from Table 1, the orthorhombic PMN–0.37PT is characterised by $d_{h}^{(1)}$ = 296 pC / N, i.e., about three times smaller than d_{h}^{*} of the related composite.

In contrast to the monotonic volume-fraction (m) dependence of the piezoelectric coefficients d_{3j}^{*} of Composite I and Composite II, their piezoelectric coefficients g_{3j}^{*} undergo extreme points at $m < 0.03$ irrespective of the Type II content and of the Euler angles. This behaviour is accounted for by the combination of the piezoelectric and dielectric properties in the composite [6] and, as a consequence, by the strong influence of the dielectric permittivity $\varepsilon_{33}^{*\sigma}$ on the piezoelectric coefficients g_{3j}^{*}. Fig. 5, a and b are built for the volume fraction m = 0.10: at this volume fraction of the PMN–0.37PT SC, we state the still high level of the longitudinal piezoelectric sensitivity, i.e., $g_{33}^{*} \approx 100$ mV·m / N. The piezoelectric coefficient g_{33}^{*} decreases (Fig. 5, a and b) at the rotation of the main crystallographic axes by the Euler angle θ, and this correlates with decreasing d_{33}^{*} in Fig. 4, d and e. The hydrostatic parameters of Composite II show the considerable dependence on the volume fraction m and Euler angle θ, see Fig. 5, c and d. In Fig. 5, c and d, we observe the correlation between g_{h}^{*} and $(Q_{h}^{*})^2$: in the present volume-fraction range m ≤ 0.10, the piezoelectric coefficient g_{h}^{*} is characterised by the non-monotonic behaviour and influences the squared figure of merit $(Q_{h}^{*})^2$ stronger than d_{h}^{*} from Eq. (7). As follows from Table 4, the correlation between g_{h}^{*} and $(Q_{h}^{*})^2$ takes place also at variations of the volume fractions of the SC components m and m_i in the composite where no rotation of the main crystallographic axes is performed in the Type I layer. Data from Table 4 show that changes in

the volume fraction of the LBO SC m_i lead to minor changes in the hydrostatic parameters at the volume fraction of the PMN–0.37PT SC m = const. In contrast to this, changes in m at m_i = const cause considerable changes in both the hydrostatic parameters. This is accounted for by a large difference between the dielectric properties of the SC components, see Tables 1 and 2. The changes in m_i mean minor changes in the dielectric permittivity $\varepsilon_{33}^{*\sigma}$ of the composite due to the small permittivity of the LBO SC. The changes in m cause considerable changes in $\varepsilon_{33}^{*\sigma}$ of the composite irrespective of m_i because of the large permittivity of the PMN–0.37PT SC.

We note the high level of the g_h^* and $(Q_h^*)^2$ values related to Composite II at $m \le 0.20$ (see Fig. 5, c and d and Table 4). For example, the values of $(Q_h^*)^2 \sim 10^{10}$ Pa^{-1} are a few times larger than those related to piezo-active composites based on FE ceramics [24] and comparable to the $(Q_h^*)^2$ values related to some composites based on relaxor-FE SCs [1, 6–8].

The piezoelectric properties of Composite II are also characterised by the large anisotropy. In Fig. 6 we show regions where the anisotropy factors from Eqs. (8) obey conditions

$$| \zeta_{d1} | \ge 5 \text{ and } | \zeta_{d2} | \ge 5 \qquad (9)$$

simultaneously. We again show the example of the composite with the relatively small volume fraction of the PMN–0.37PT SC (m = 0.10 as noted in Fig. 5), i.e., the composite wherein the Type II layer strongly influences the piezoelectric anisotropy due to the elastic anisotropy (see Table 3). Validity of inequalities (9) mean that a conversion of electric energy into mechanical energy and vice versa proceeds mainly along the OX_3 direction concerned with the large piezoelectric coefficient d_{33}^*. Based on areas 1 and 2 in Fig. 6, we state that the rotations of the main crystallographic axes of the SC component in the Type I layer by the Euler angles ψ and θ also influence the piezoelectric anisotropy of Composite II. Hereby changes in the Euler angle φ influence the piezoelectric anisotropy to a lesser degree. Earlier we observed the weak influence of the rotation by φ on the longitudinal piezoelectric effect in Composite II, see Fig. 4, d and e, and Fig. 5, a and b. In our opinion, such a mode of rotation plays the passive role in Composite II

because the $\boldsymbol{P}_s^{(1)}$ orientation in its Type II layer remains unchanged with respect to the OX_3 axis (Fig. 1). We add that Composite II has obvious advantages over the conventional $PbTiO_3$-type FE ceramics with the large piezoelectric anisotropy [23] because validity of conditions (9) is observed at the piezoelectric coefficient d_{33}^* that is about an order-of-magnitude larger than d_{33} of the highly anisotropic $PbTiO_3$-type ceramics with $d_{33} < 100$ pC / N.

4. Conclusions

The present paper reports results on the piezoelectric performances of Composite I and Composite II with two SC components. These materials are characterised by 2–0–2 connectivity and by the presence of the single-domain relaxor-FE SC as a main piezoelectric component. This component is either tetragonal (in Composite I) or orthorhombic (in Composite II) and forms the Type I layers in the sample (Fig. 1). In the Type II layer that is regarded as a 0–3 composite, an important combination of the properties is achieved due to the LBO SC with the unusual anisotropy of the properties, see Table 2. The Type II layer with the considerable elastic anisotropy strongly influences the piezoelectric performance of Composite I and Composite II. Such an influence of the Type II layer and the orientation effect in the Type I layer enables us to improve the hydrostatic piezoelectric response of the studied composites, especially Composite II (see Figs. 3, 4, a and c, 5, c and d). The large piezoelectric anisotropy in Composite II is also observed due to the orientation effect in the Type I layer and the elastic anisotropy in the Type II layer. Validity of conditions (9) is observed at $d_{33}^* \sim 10^2$ pC / N that represents obvious advantages over the conventional $PbTiO_3$-type FE ceramics.

The sets of large values of the studied piezoelectric coefficients and hydrostatic parameters, and anisotropy factors (Figs. 3–5) make Composite II more preferable in comparison to Composite I and suggest that Composite II can be effective in hydroacoustic, piezoelectric sensor and energy-harvesting applications.

Acknowledgements

The authors would like to thank Prof. Dr. A. A. Nesterov, Prof. Dr. A. E. Panich, and Prof. Dr. I. A. Parinov (Southern Federal University, Russia), and Prof. Dr. L. N. Korotkov (Voronezh State Technical University, Russia) for their interest in the research problem. Prof. Dr. C. R. Bowen acknowledges funding from the European Research Council under the European Union's Seventh Framework Programme (FP/2007-2013) / ERC Grant Agreement no.320963 on Novel Energy Materials, Engineering Science and Integrated Systems (NEMESIS). Research has been carried out at the financial support from the Ministry of Education and Science of the Russian Federation within the framework of the complex project “Working out and creation of a high-technological production of a mobile hydroacoustic complex to highlight a situation in various areas of the World ocean on the basis of modern piezoelectric means of the new generation” (contract No. 03.G25.31.0276, May 29th, 2017) by using the equipment of the Centre of Collective Use “High Technologies” at the Southern Federal University.

References

1. S. Zhang, F. Li, High performance ferroelectric relaxor-$PbTiO_3$ single crystals: Status and perspective, *J. Appl. Phys.* **111**, 031301 (2012).
2. S. Zhang, F. Li, J. Luo, R. Sahul, T. R. Shrout, Relaxor-$PbTiO_3$ single crystals for various applications, *IEEE Trans. Ultrason., Ferroelec., Freq. Contr*. **60**, 1572 (2013).
3. R. Zhang, B. Jiang, W. Cao, Elastic, piezoelectric, and dielectric properties of multidomain $0.67Pb(Mg_{1/3}Nb_{2/3})O_3$–$0.33PbTiO_3$ single crystals, *J. Appl. Phys*. **90**, 3471 (2001).
4. L. Zheng, Y. Jing, X. Lu, R. Wang, G. Liu, W. Lű, R. Zhang, W. Cao, Temperature and electric-field induced phase transitions, and full tensor properties of $[011]_C$-poled domain-engineered tetragonal $0.63Pb(Mg_{1/3}Nb_{2/3})O_3$-$0.37PbTiO_3$ single crystals, *Phys Rev B* **93**, 094104 (2016).
5. F. Wang, C. He, Y. Tang, Single crystal $0.7Pb(Mg_{1/3}Nb_{2/3})O_3$–$0.3PbTiO_3$ / epoxy 1–3 piezoelectric composites prepared by the lamination technique, *Mater. Chem. Phys*. **105**, 273 (2007).
6. V. Yu. Topolov, P. Bisegna, and C. R. Bowen, *Piezo-Active Composites. Orientation Effects and Anisotropy Factors* (Springer, Berlin, Heidelberg, 2014).
7. C. R. Bowen, V. Yu. Topolov, A. N. Isaeva, P. Bisegna, Advanced composites based on relaxor-ferroelectric single crystals: from electromechanical coupling to energy-harvesting applications, *CrystEngComm* **18**, 5986 (2016).
8. V. Yu. Topolov, C. R. Bowen, P. Bisegna, *Piezo-Active Composites. Microgeometry – Sensitivity Relations* (Springer International, Cham, 2018).
9. R. Zhang, B. Jiang, W. Cao, Single-domain properties of $0.67Pb(Mg_{1/3}Nb_{2/3})O_3$-$0.33PbTiO_3$ single crystals under electric field bias, *Appl. Phys. Lett.* **82**, 787 (2003).
10. G. Liu, W Jiang, J. Zhu, W. Cao, Electromechanical properties and anisotropy of single and multi-domain $0.72Pb(Mg_{1/3}Nb_{2/3})O_3$−$0.28PbTiO_3$ single crystals, *Appl. Phys. Lett.* **99**, 162901 (2011).

11. Y. Jing, L. Zheng, W. Lű, Z. Xi, P. Zheng, J. Du, R. Zhang, Full tensor properties of single-domain tetragonal $0.63Pb(Mg_{1/3}Nb_{2/3})O_3–0.37PbTiO_3$ single crystal and their orientation dependence, *Phys. Stat. Sol. B* **253**, 1994 (2016).

12. R. Zhang, W. Jiang, B. Jiang, W. Cao, Elastic, dielectric and piezoelectric coefficients of domain engineered $0.70Pb(Mg_{1/3}Nb_{2/3})O_3$-$0.30PbTiO_3$ single crystal, In: Cohen RE (ed.) *Physics of Ferroelectrics* (American Institute of Physics, Melville, 2002), p.188.

13. X. Dongyu, C. Xin, H. Shifeng, Investigation of inorganic fillers on properties of 2–2 connectivity cement / polymer based piezoelectric composites, *Constr. Build. Mater*. **94**, 678 (2015).

14. V. Yu. Topolov, C. R. Bowen, I. A. Ermakov, Remarkable hydrostatic piezoelectric response of novel 2–0–2 composites, *Ferroelectrics. Lett. Sec*. **43**, 90 (2016).

15. V. Yu. Topolov, C. R. Bowen, A. V. Krivoruchko, Piezoelectric performance and hydrostatic parameters of novel 2–2-type composites, *IEEE Trans. Ultrason., Ferroelec., Freq. Contr*. **64**, 1599 (2017).

16. V. Yu. Topolov, C. R. Bowen, A. A. Panich, A. N. Isaeva, Piezoelectric sensitivity and hydrostatic response of novel lead-free 2–0–2 composites with two single-crystal components, *Mater. Chem. Phys*. **201**, 224 (2017).

17. R. E. Newnham, D. P. Skinner, L. E. Cross, Connectivity and piezoelectric-pyroelectric composites, *Mater. Res. Bull*. **13**, 525 (1978).

18. J. H. Huang, S. Yu, Electroelastic Eshelby tensors for an ellipsoidal piezoelectric inclusion, *Composites Engineering* 4, 1169 (1994).

19. T. Ikeda, *Fundamentals of Piezoelectricity* (Oxford University Press, Oxford, New York, Toronto, 1990).

20. M. Adachi, T. Shiosaki, H. Kobayashi, O. Ohnishi, A. Kawabata, Temperature compensated piezoelectric lithium tetraborate crystal for high frequency surface acoustic

wave and bulk wave device applications, In: *Proceedings of 1985 IEEE Ultrasonics Symposium* (IEEE, New York, 1985), p. 228.

21. K. E. Evans, K. L. Alderson, The static and dynamic moduli of auxetic microporous polyethylene, *J. Mater. Sci. Lett*. **11**, 1721 (1992).
22. I. N. Groznov, Dielectric permittivity, In: *Physics Encyclopaedia* (Sovetskaya Entsiklopediya, Moscow, 1983, in Russian), p. 178.
23. Y. Xu, *Ferroelectric Materials and Their Applications* (North-Holland, Amsterdam, London, New York, Toronto, 1991).
24. E. K. Akdogan, M. Allahverdi, A. Safari, Piezoelectric composites for sensor and actuator applications, *IEEE Trans. Ultrason., Ferroelec., Freq. Contr*. **52,** 746 (2005).

To the paper "Domain orientations and piezoelectric properties in novel 2–2-type composites with two single-crystal components" by V. Yu. Topolov, A. V. Krivoruchko, C. R. Bowen, and A. A. Panich

Table 1. Room-temperature elastic compliances s_{ab}^{E} (in 10^{-12} Pa^{-1}) at electric field E = const, piezoelectric coefficients d_{ij} (in pC / N) and relative dielectric permittivities $\varepsilon_{pp}^{\sigma} / \varepsilon_0$ at mechanical stress σ = const of single-domain PMN–0.37PT SCs

Electromechanical constants	[001]-poled PMN–0.37PT SC [11], 4*mm* symmetry	[011]-poled PMN–0.37PT SC [4], *mm*2 symmetry
s_{11}^{E}	12.21	20.5
s_{12}^{E}	–0.09	–10.5
s_{13}^{E}	–9.61	–14.0
s_{22}^{E}	12.21	12.6
s_{23}^{E}	–9.61	3.6
s_{33}^{E}	24.1	20.0
s_{44}^{E}	33.78	18.9
s_{55}^{E}	33.78	4.2
s_{66}^{E}	15.72	32.8
d_{15}	1410	120
d_{24}	1410	645
d_{31}	–130	–960
d_{32}	–130	204
d_{33}	307	1052
$\varepsilon_{11}^{\sigma} / \varepsilon_0$	12550	2197
$\varepsilon_{22}^{\sigma} / \varepsilon_0$	12550	6803
$\varepsilon_{33}^{\sigma} / \varepsilon_0$	775	10661

Table 2. Room-temperature elastic moduli c_{ab}^{E} (in 10^{10} Pa), piezoelectric coefficients e_{ij} (in C / m^2) and relative dielectric permittivities $\varepsilon_{pp}^{\xi} / \varepsilon_0$ at mechanical strain ξ = const of components of the Type II layer

Electromechanical constants	LBO SC [20], 4*mm* symmetry	Polyethylene [21, 22], isotropic
c_{11}^{E}	13.5	0.0778
c_{12}^{E}	0.357	0.0195
c_{13}^{E}	3.35	0.0195
c_{33}^{E}	5.68	0.0778
c_{44}^{E}	5.85	0.0292
c_{66}^{E}	4.67	0.0292
e_{15}	0.472	0
e_{31}	0.290	0
e_{33}	0.928	0
$\varepsilon_{11}^{\xi} / \varepsilon_0$	8.90	2.3
$\varepsilon_{33}^{\xi} / \varepsilon_0$	8.07	2.3

Table 3. Aspect-ratio dependence of elastic compliances $s_{ab}^{(2),E}$ (in 10^{-12} Pa^{-1}) of the 0–3 LBO SC / polyethylene composite at m_i = 0.10 [16]

ρ_i	$s_{11}^{(2),E}$	$s_{12}^{(2),E}$	$s_{13}^{(2),E}$	$s_{33}^{(2),E}$
1	112	–18.7	–26.5	118
5	85.7	–10.7	–22.8	128
10	74.4	–6.50	–20.2	128
50	59.9	–1.08	–16.8	126
100	57.6	–0.218	–16.2	126

Table 4. Hydrostatic piezoelectric coefficient g_h^* (in mV·m / N) and squared figure of merit $(Q_h^*)^2$ (in 10^{-12} Pa^{-1}) of Composite II at $\rho_i = 100$ and $\varphi = \psi = \theta = 0°$

m_i \ m	0.05	0.10	0.15	0.20
g_h^*				
0.05	187	187	185	183
0.10	99.8	100	99.5	98.3
0.15	66.4	67.1	66.8	66.2
0.20	48.8	49.4	48.3	42.8
$(Q_h^*)^2$				
0.05	140	141	144	131
0.10	86.2	86.5	84.5	82.0
0.15	59.0	59.9	58.9	57.6
0.20	43.0	44.0	43.6	42.9

Figure captions to the paper “Domain orientations and piezoelectric properties in novel 2–2-type composites with two single-crystal components” by V. Yu. Topolov, A. V. Krivoruchko, C. R. Bowen, and A. A. Panich

Fig. 1. Schematic of the 2–2-type composite with the parallel connection of the layers. The Type II layer represents the 0–3 SC / polymer composite.

Fig. 2. Piezoelectric coefficients d_{3j}^{*} and d_{h}^{*} of Composite I at the rotation of the main crystallographic axes of the tetragonal PMN–0.37PT SC by the Euler angle θ.

Fig. 3. Piezoelectric coefficients d_{3j}^{*} and d_{h}^{*} of Composite II at φ = ψ = θ = 0°.

Fig. 4. Piezoelectric coefficients d_{h}^{*} (a–c) and d_{33}^{*} (d and e) of Composite II at the rotation of the main crystallographic axes of the orthorhombic PMN–0.37PT SC by the Euler angles φ, ψ, and θ.

Fig. 5. Piezoelectric coefficients g_{33}^{*} (a and b) and g_{h}^{*} (c), and squared hydrostatic figure of merit $(Q_{h}^{*})^2$ (d) of Composite II at the rotation of the main crystallographic axes of the orthorhombic PMN–0.37PT SC by the Euler angles φ, ψ, and θ.

Fig. 6. Regions of validity of conditions $|\zeta_{d1}| \geq 5$ and $|\zeta_{d2}| \geq 5$ in Composite II.

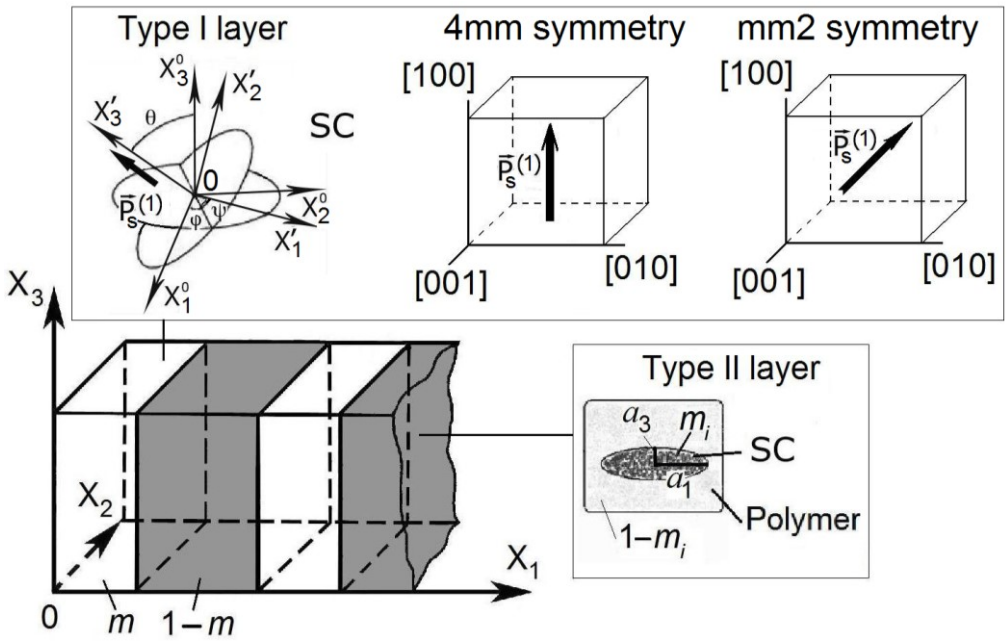
Type I layer
4mm symmetry
mm2 symmetry
SC
[100]
[001]
[010]
Type II layer
Polymer
0
m
1−m

Fig. 1

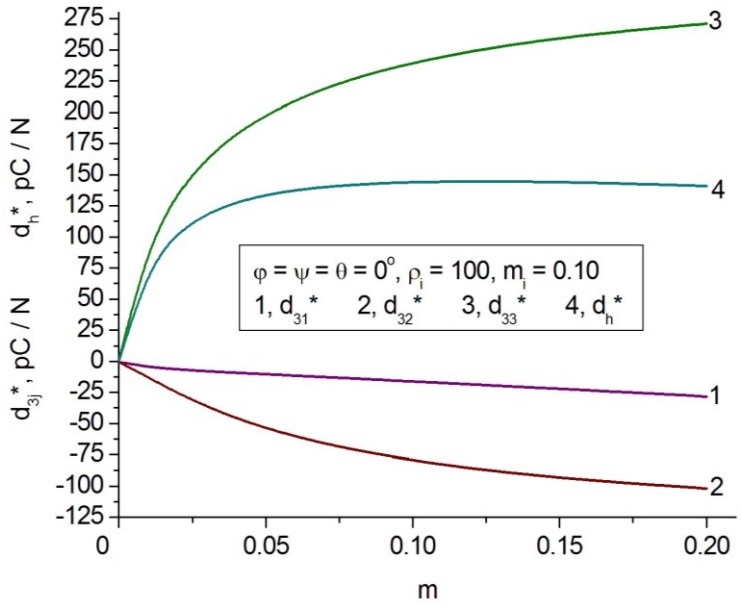
275
250
225
200
175
150
125
100
75
50
25
0
-25
-50
-75
-100
-125
0
0.05
0.10
0.15
0.20
m
d_h^*, pC / N
d_{3j}^*, pC / N
φ = ψ = θ = 0°, ρ_i = 100, m_i = 0.10
1, d_{31}^* 2, d_{32}^* 3, d_{33}^* 4, d_h^*
1
2
3
4

a

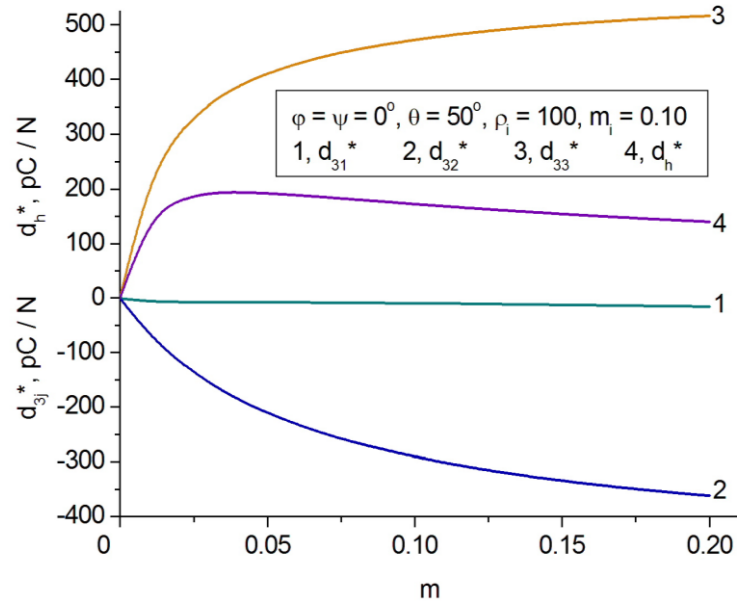
500
400
300
200
100
0
-100
-200
-300
-400
0
0.05
0.10
0.15
0.20
m
d_h^*, pC / N
d_{3j}^*, pC / N
φ = ψ = 0°, θ = 50°, ρ_i = 100, m_i = 0.10
1, d_{31}^* 2, d_{32}^* 3, d_{33}^* 4, d_h^*
1
2
3
4

b

Fig. 2

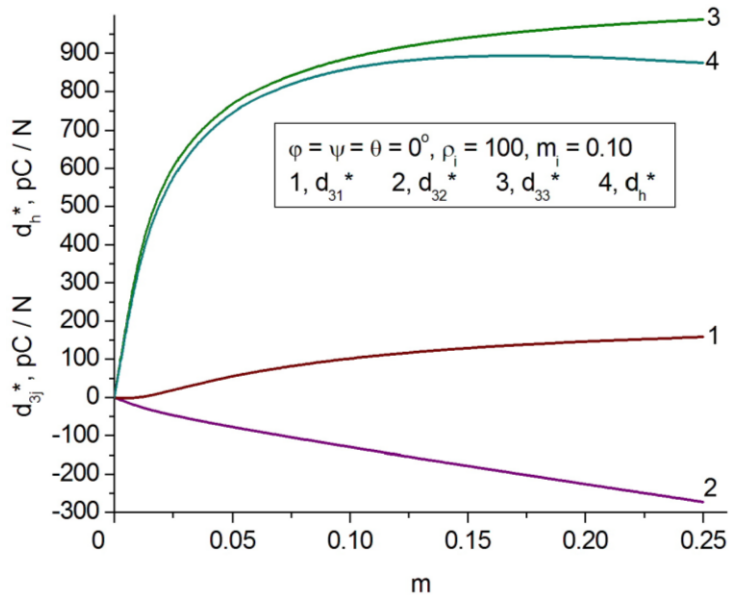
3
4
1
2
φ = ψ = θ = 0°, ρi = 100, mi = 0.10
1, d31* 2, d32* 3, d33* 4, dh*
dh*, pC / N
d3j*, pC / N
900
800
700
600
500
400
300
200
100
0
-100
-200
-300
0
0.05
0.10
0.15
0.20
0.25
m

Fig. 3

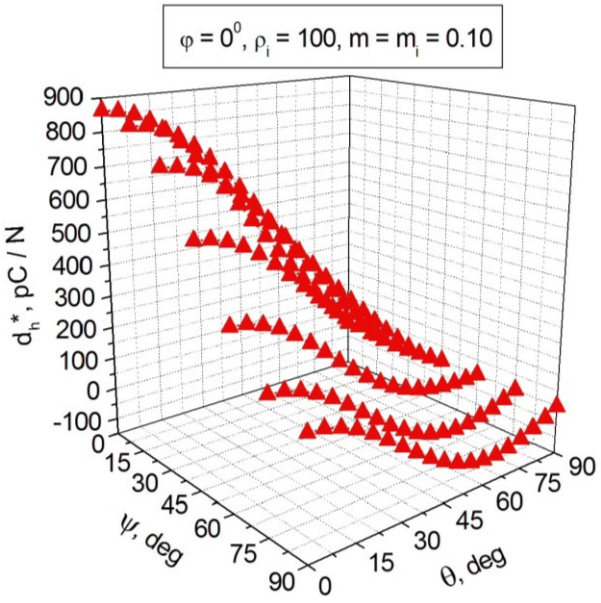
φ = 0⁰, ρi = 100, m = mi = 0.10
dh*, pC / N
ψ, deg
θ, deg

a

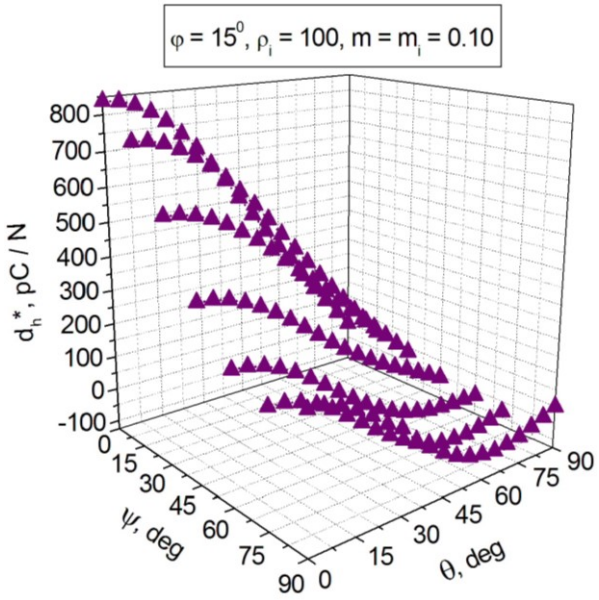
φ = 15⁰, ρi = 100, m = mi = 0.10
dh*, pC / N
ψ, deg
θ, deg

b

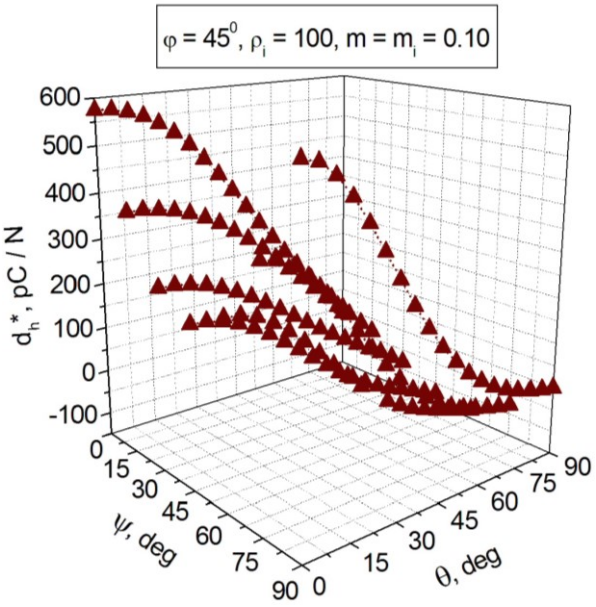
φ = 45⁰, ρi = 100, m = mi = 0.10
dh*, pC / N
ψ, deg
θ, deg

c

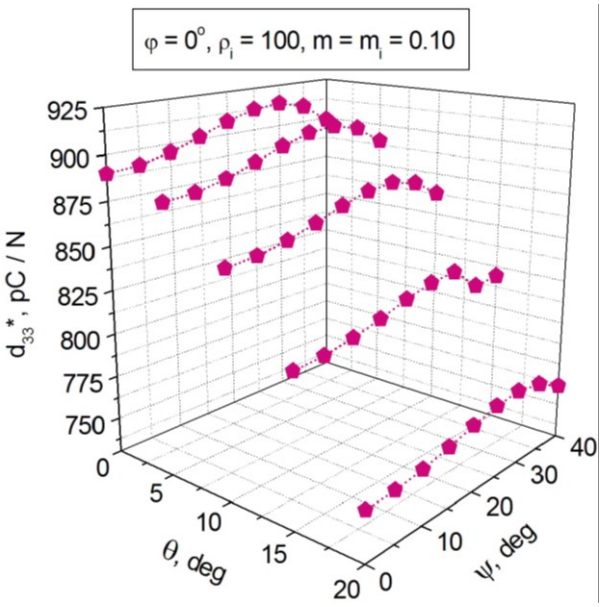
φ = 0°, ρi = 100, m = mi = 0.10
d33*, pC / N
θ, deg
ψ, deg

d

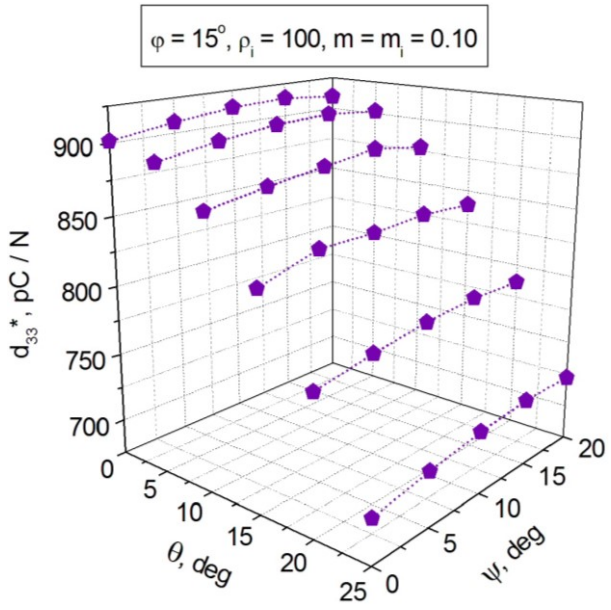
φ = 15°, ρi = 100, m = mi = 0.10
d33*, pC / N
θ, deg
ψ, deg

e

Fig. 4

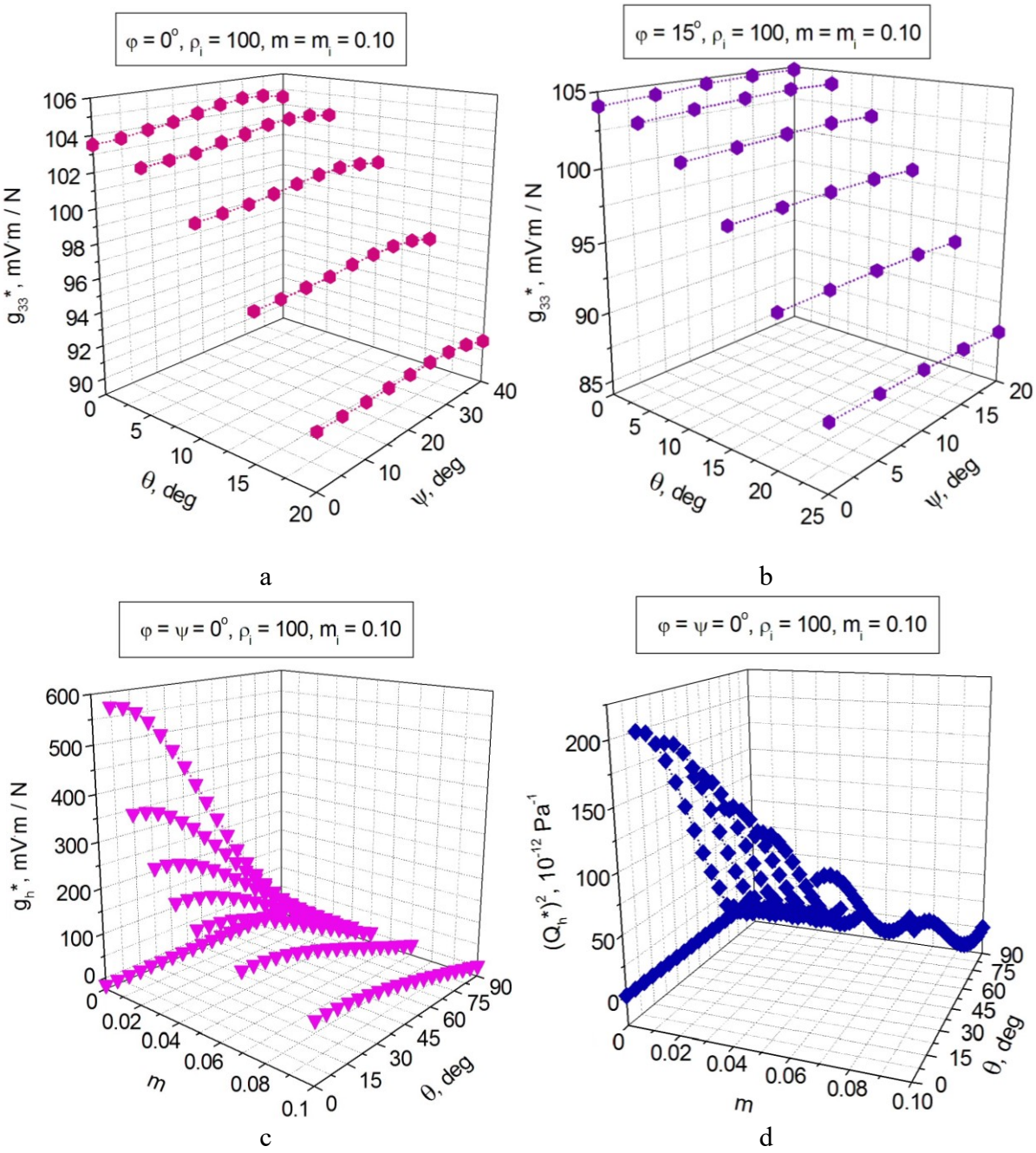
φ = 0°, ρi = 100, m = mi = 0.10
g33*, mV m / N
θ, deg
ψ, deg
a
φ = 15°, ρi = 100, m = mi = 0.10
g33*, mV m / N
θ, deg
ψ, deg
b
φ = ψ = 0°, ρi = 100, mi = 0.10
gh*, mV m / N
m
θ, deg
c
φ = ψ = 0°, ρi = 100, mi = 0.10
(Qh*)2, 10-12 Pa-1
m
θ, deg
d

Fig. 5

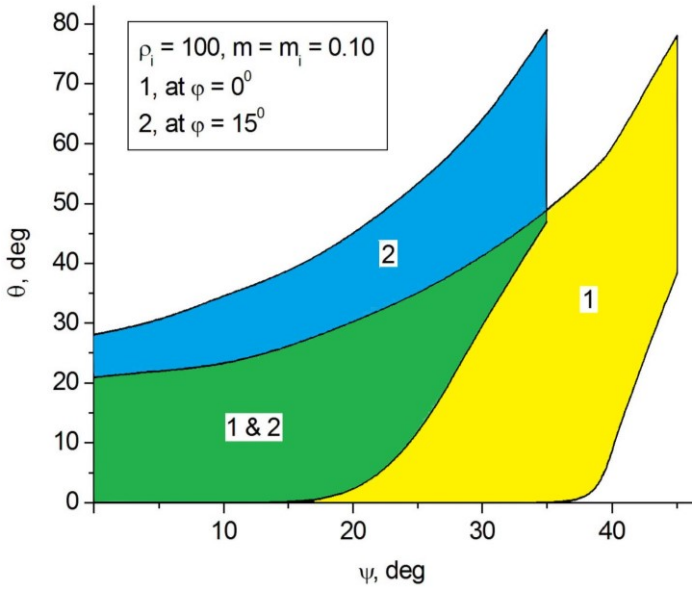
ρi = 100, m = mi = 0.10
1, at φ = 0⁰
2, at φ = 15⁰
θ, deg
ψ, deg
1
2
1 & 2
0
10
20
30
40
50
60
70
80

Fig. 6